Nuclear Engineering and Design 49 (1978) 231–241

PLASTEF: A CODE FOR THE NUMERICAL SIMULATION OF THERMOELASTOPLASTIC BEHAVIOUR OF MATERIALS USING THE FINITE ELEMENT METHOD

Fernando G. BASOMBRÍO and G. SÁNCHEZ SARMIENTO
Centro Atómico Bariloche, Comisión Nacional de Energía Atómica. 8400 – San Carlos de Bariloche, R.N., Argentina

Received 18 February 1978

A general code for solving two-dimensional thermo-elastoplastic problems in geometries of arbitrary shape using the finite element method, is presented. The initial stress incremental procedure was adopted, for given histories of load and temperature. Some classical applications are included.

1. Introduction

A general code whose purpose is to simulate the thermo-elastoplastic behaviour of materials using the finite element method is presented. Technological problems of arbitrary shape can be solved for plane stress and strain, or symmetry of revolution, for given histories of loads and temperatures, and for any strain-hardening law. Spontaneous unloadings on any point of the material are automatically taken into consideration.

A review of some of the publications preceeding this paper is presented in references [1] to [19]. We have followed more closely the line of Zienkiewicz and co-workers [3–5]. The program is based on the incremental method of initial stresses and for each increment of load, stresses satisfying the equilibrium conditions are stored. The Levy–Mises–Prandtl–Reuss equations were adopted [20].

The code was intensively tested and some of the classical problems solved are included in the last section.

2. Usual expressions of the theory of plasticity

This classical theory for isotropic materials with isotropic strain hardening [20] has been frequently reformulated for computational purposes [1–4, 13–17,21] and also extended to cover a wide class of problems related to plasticity [5].

We now give a brief review of the fundamental expressions used in the program and refer the reader for details to the above mentioned literature.

Let $p(s), \mathcal{F}(s), T(s)$ be the given histories of external loads and temperatures parametrized with s. ($p(s)$ is the volume load, $\mathcal{F}(s)$ the surface load, and $T(s)$ the temperature spatial distribution). For each value of the parameter s we shall have in each point of the material, displacements, strains and stresses noted by $\boldsymbol{u}$, $\epsilon_{ij}(s)$ and $\sigma_{ij}(s)$. A dot over a symbol will mean derivation with respect to s.

Let $F(J'_2, J'_3, \kappa)$ be the yield function for isotropic materials, where J'_2 and J'_3 are the invariants:

$$J'_2 = \tfrac{1}{2}\sigma'_{ij}\sigma'_{ij}\,, \quad J'_3 = \tfrac{1}{3}\sigma'_{ij}\sigma'_{jk}\sigma'_{kl} \tag{1}$$

where: $\sigma'_{ij} = \sigma_{ij} - \tfrac{1}{3}\sigma_{kk}$ is the deviatoric of the stress tensor, and

$$\kappa = \kappa\left(\int \sigma_{ij}\mathrm{d}\epsilon^{\mathrm{p}}_{ij}\right)$$

is the strain hardening parameter depending on the plastic work. ($\epsilon^{\mathrm{p}}_{ij}$ is plastic part the strain tensor).

The rate of plastic strain satisfies the usual flow rule:

$$\dot{\epsilon}^{\mathrm{p}}_{ij} = \dot{\lambda}\frac{\partial F}{\partial \sigma_{ij}}, \tag{2}$$

($\dot{\lambda}$ = proportionality factor).

In the particular case of the Levy–Mises–Prandtl–Reuss theory the above expression take the form [20]:

$$F(J'_2, J'_3, \kappa) \equiv \sqrt{3J'_2} - \kappa\left(\int \overline{\sigma \mathrm{d}\epsilon^{\mathrm{p}}}\right) \equiv \bar{\sigma} - H\left(\int \overline{\mathrm{d}\epsilon^{\mathrm{p}}}\right), \tag{3}$$

with

$$\bar{\sigma} = \sqrt{\tfrac{3}{2}\sigma'_{ij}\sigma'_{ij}} = \sqrt{\tfrac{1}{2}[(\sigma_{11}-\sigma_{22})^2 + (\sigma_{22}-\sigma_{33})^2 + (\sigma_{33}-\sigma_{11})^2 + 6(\sigma_{12}^2+\sigma_{23}^2+\sigma_{31}^2)]} \tag{4}$$

and

$$\bar{\epsilon}^{\mathrm{p}} = \sqrt{\tfrac{2}{3}\epsilon_i^{\mathrm{p}}\epsilon_i^{\mathrm{p}}}\,, \quad \epsilon_i^{\mathrm{p}} = 0\,. \tag{5}$$

$H(\int \overline{\mathrm{d}\epsilon^{\mathrm{p}}})$ is the equivalent stress/plastic strain curve of the conventional uniaxial test.

The final expression is [2]:

$$\dot{\sigma}_{ij} = 2G\left(\dot{\epsilon}_{ij} + \frac{\nu}{1-2\nu}\delta_{ij}\dot{\epsilon}_{ii} - \mu\sigma'_{ij}\frac{\sigma'_{kl}\dot{\epsilon}_{kl}}{S}\right), \tag{6}$$

where ν = Poisson coefficient, G = shear modulus, $S = \frac{2}{3}\bar{\sigma}^2(1 + H'/3G)$, H': slope of the curve H, and

$$\mu = \mu(\sigma_{ij}, \kappa, \dot{\sigma}_{ij}, \dot{\kappa}) = \begin{cases} 0, \text{ if } \begin{cases} \dot{F}(\sigma_{ij}, \kappa, \dot{\sigma}_{ij}, \dot{\kappa}) < 0 \\ \text{or } F < 0 \end{cases} \\ 1, \text{ if } \begin{cases} \dot{F} \geqslant 0 \\ \text{and } F = 0\,. \end{cases} \end{cases} \tag{7}$$

Introducing now the more convenient vector notation:

$$\boldsymbol{\varepsilon} = \begin{bmatrix} \epsilon_{11} \\ \epsilon_{22} \\ \epsilon_{33} \\ \epsilon_{12} \\ \epsilon_{13} \\ \epsilon_{23} \end{bmatrix}, \quad \boldsymbol{\sigma} = \begin{bmatrix} \sigma_{11} \\ \sigma_{22} \\ \sigma_{33} \\ \sigma_{12} \\ \sigma_{23} \\ \sigma_{31} \end{bmatrix}, \tag{8}$$

eq. (6) may be rewritten as [2,1]:

$$\dot{\boldsymbol{\sigma}} = \mathbf{D}^{\mathrm{ep}}(\dot{\boldsymbol{\varepsilon}} - \dot{\boldsymbol{\varepsilon}}^{\theta})\,, \tag{9}$$

if the thermal strain $\boldsymbol{\varepsilon}^{\theta}$ are included, being the elastic constant independent of the temperature [12–15], where

$$\mathbf{D}^{\mathrm{ep}} = \mathbf{D}^{\mathrm{el}} + \mu\mathbf{D}^{\mathrm{pl}} \tag{10}$$

is the elasto-plastic matrix [1,2,3], and

$$\mathbf{D}^{\mathrm{el}} = \frac{E}{1+\nu}$$

$$\times \begin{bmatrix} \frac{1-\nu}{1-2\nu} & & & & & \\ \frac{\nu}{1-2\nu} & \frac{1-\nu}{1-2\nu} & & & & \\ \frac{\nu}{1-2\nu} & \frac{\nu}{1-2\nu} & \frac{1-\nu}{1-2\nu} & & & \\ 0 & 0 & 0 & \frac{1}{2} & & \\ 0 & 0 & 0 & 0 & \frac{1}{2} & \\ 0 & 0 & 0 & 0 & 0 & \frac{1}{2} \end{bmatrix} \tag{11}$$

$$\mathbf{D}^{\mathrm{pl}} = -\frac{E}{(1+\nu)S}$$

$$\times \begin{bmatrix} \sigma'^2_{11} & & & & & \\ \sigma'_{11}\sigma'_{22} & \sigma'^2_{22} & & & & \\ \sigma'_{11}\sigma'_{33} & \sigma'_{22}\sigma'_{33} & \sigma'^2_{33} & & & \\ \sigma'_{11}\sigma_{12} & \sigma'_{22}\sigma_{12} & \sigma'_{33}\sigma_{12} & \sigma^2_{12} & & \\ \sigma'_{11}\sigma_{23} & \sigma'_{22}\sigma_{23} & \sigma'_{33}\sigma_{23} & \sigma_{12}\sigma_{23} & \sigma^2_{23} & \\ \sigma'_{11}\sigma_{31} & \sigma'_{22}\sigma_{31} & \sigma'_{33}\sigma_{31} & \sigma_{12}\sigma_{31} & \sigma_{23}\sigma_{31} & \sigma^2_{31} \end{bmatrix}. \tag{12}$$

(E is Young's modulus).

3. Finite element discretization

For the finite elements discretization of the two-dimensional continuum, we designate:

U = vector of nodal displacements,

U^e = vector of nodal displacements of the element e, and

u = displacements field within the element e.

The usual linear relation [4] hold

$$u = \mathbf{N}U^e \qquad \boldsymbol{\varepsilon} = \mathbf{B}U^e \tag{13}$$

where $\mathbf{N}$ is the matrix of shape functions, and $\mathbf{B}$ is the matrix relating the vector of nodal displacements with the strain vector.

The standard application of the virtual work principle to the discretized problem (Galerkin method) leads to the following non-linear system of algebraic equations for the nodal displacements rate, making

use of eq. (9):

$$\mathbf{A}\dot{U} = R\,, \tag{14}$$

where

$$A(\sigma, \kappa, \dot{\sigma}, \dot{\kappa}, \dot{U}) = \text{''}\sum_{e}\text{''}\left\{\int_{e}\mathbf{B}^{\mathrm{T}}\mathbf{D}^{\mathrm{ep}}\mathbf{B}\mathrm{d}\nu - \int_{\lambda}k\mathbf{N}\mathbf{N}^{\mathrm{T}}\mathrm{d}\sigma\right\}, \tag{15}$$

$$R = \text{''}\sum_{e}\text{''}\left\{\int_{e}\mathbf{N}^{\mathrm{T}}\dot{p}\mathrm{d}\nu + \int_{\lambda}\mathbf{N}^{\mathrm{T}}\dot{\mathcal{F}}\mathrm{d}\sigma + \int_{e}\mathbf{B}^{\mathrm{T}}\mathbf{D}^{\mathrm{ep}}\dot{\epsilon}^{\theta}\mathrm{d}\nu\right\}, \tag{16}$$

and

$\text{''}\sum_{e}\text{''}$ = the general assembly starting from the element contributions,
e = an element,
$\mathbf{B}^{\mathrm{T}}$ = the transpose of the matrix $\mathbf{B}$,
k = the coefficient of the elastic boundary reaction,
λ = the side of the element "e" where boundary contributions exist,
$\mathrm{d}\nu$ = an element of volume, and
$\mathrm{d}\sigma$ = an element of arc.

4. Iterative resolution of the non-linear algebraic equations

With the aim of obtaining the expressions corresponding to the "initial stress method" (Newton–Raphson algorithm with constant slope [4]), we reformulate the preceeding equations using eqs. (10) and (13):

$$\hat{\mathbf{A}}\dot{U} = \hat{R}\,, \tag{17}$$

$$\hat{\mathbf{A}} = \text{''}\sum_{e}\text{''}\left\{\int_{e}\mathbf{B}^{\mathrm{T}}\mathbf{D}^{\mathrm{el}}\mathbf{B}\mathrm{d}\nu - \int_{\lambda}k\mathbf{N}^{\mathrm{T}}\mathbf{N}\mathrm{d}\sigma\right\}, \tag{18}$$

$$\hat{R}(\sigma, \kappa, \dot{\sigma}, \dot{\kappa}, \dot{U}) = R' + R''(\sigma, \kappa, \dot{\sigma}, \dot{\kappa}, \dot{U})\,, \tag{19}$$

$$R' = \text{''}\sum_{e}\text{''}\left\{\int_{e}\mathbf{N}^{\mathrm{T}}\dot{p}\mathrm{d}\nu + \int_{\lambda}\mathbf{N}^{\mathrm{T}}\dot{\mathcal{F}}\mathrm{d}\sigma + \int_{e}\mathbf{B}^{\mathrm{T}}\mathbf{D}^{\mathrm{el}}\dot{\epsilon}^{\theta}\mathrm{d}\nu\right\}, \tag{20}$$

$$R''(\sigma, \kappa, \dot{\sigma}, \dot{\kappa}, \dot{U}) = -\text{''}\sum_{e}\text{''}\int_{e}\mathbf{B}^{\mathrm{T}}\dot{\sigma}_{\mathrm{ini}}\mathrm{d}\nu\,, \tag{21}$$

$$\dot{\sigma}_{\mathrm{ini}} = \mu\mathbf{D}^{\mathrm{pl}}(\dot{\varepsilon} - \dot{\varepsilon}^{\theta})\,, \quad \text{(initial stresses)} \tag{22}$$

where the non-linear part of the rigidity matrix $\mathbf{A}$ has been shifted to the right hand side of eq. (17).

The iterative process consists on doing succesive trials on the initial stresses $\dot{\sigma}_{\mathrm{ini}}$ in eqs. (21), (22). The generic iteration i may be written as

$$\hat{\mathbf{A}}\dot{U}^{i} = \hat{R}^{i}\,, \quad \dot{U}^{i} = \hat{\mathbf{A}}^{-1}\hat{R}^{i}\,, \tag{23}$$

$$\hat{R}^{i} = R' + R''^{i}\,, \tag{24}$$

$$R''^{i} = -\text{''}\sum_{e}\text{''}\int_{e}\mathbf{B}^{\mathrm{T}}\dot{\sigma}^{i}_{\mathrm{ini}}\mathrm{d}\nu\,, \tag{25}$$

$$\dot{\sigma}^{i}_{\mathrm{ini}} = \mu^{i-1}\mathbf{D}^{\mathrm{pl}}(\dot{\varepsilon}^{i-1} - \dot{\varepsilon}^{\theta}) = \dot{\sigma}^{i-1}_{\mathrm{r}} + \dot{\sigma}^{i-1}_{\mathrm{ini}}\,, \tag{26}$$

$$\dot{\sigma}^{i-1}_{\mathrm{r}} = \mathbf{D}^{\mathrm{ep}}(\dot{\varepsilon}^{i-1} - \dot{\varepsilon}^{\theta}) - \dot{\sigma}^{i-1}\,, \tag{27}$$

$$\mu^{i-1} = \mu(\sigma, \kappa, \dot{\sigma}^{i-1}, \dot{\kappa}^{i-1})\,. \tag{28}$$

The algorithm may be accelerated if instead of eq. (26) we use

$$\dot{\sigma}^{i}_{\mathrm{ini}} = \omega\dot{\sigma}^{i-1}_{\mathrm{r}} + \dot{\sigma}^{i-1}_{\mathrm{ini}} \tag{26'}$$

being ω an acceleration factor.

In practice the equations are solved in an incremental manner according to the prescribed histories of loads and temperature. We replace in eqs. (23)–(28) $\dot{\varepsilon}, \dot{\sigma}, \dot{\sigma}_{\mathrm{ini}}, \dot{\sigma}_{\mathrm{r}}$, etc., by

$$s_n = \sum_{m=1}^{n}\Delta s_m\,, \quad \Delta\varepsilon_n = \dot{\varepsilon}\Delta s_n$$

$$\Delta\sigma_n = \dot{\sigma}\Delta s_n\,, \quad \sigma_{\mathrm{ini}_n} = \dot{\sigma}_{\mathrm{ini}}\Delta s_n\,, \tag{29}$$

$$\sigma_{r_n} = \dot{\sigma}_{\mathrm{r}}\Delta s_n\,, \quad \text{etc.}$$

ignoring the common divisor s_n.

The iterative algorithm eqs. (23)–(28) may begin ($i = 0$) with:

$$\sigma^{0}_{\mathrm{ini}_n} = \sigma^{\infty}_{\mathrm{ini}_{n-1}} \equiv \sigma_{\mathrm{ini}_{n-1}} \qquad (\sigma^{\infty}_{\mathrm{ini}_0} = 0)$$

$$\mu^{0}_{n} = \mu^{\infty}_{n-1} \equiv \mu_{n-1}\,, \tag{30}$$

where the index ∞ means the limit when $i \to \infty$, or in the program, the last iteration of the former load increment.

We can rewrite eq. (23–28) in a more compact and usual form [4,5]. For simplicity it is assumed that the second member $\hat{R}$ is only a function of the unknown vector $\dot{U}$. Then we put:

$$\hat{\mathbf{A}}\dot{U}^{i} = \hat{R}^{i} = \hat{R}(\dot{U}^{i-1})\,, \tag{23}$$

$$\psi(X) \equiv \hat{\mathbf{A}}X - \hat{R}(X)\,, \quad \psi(\dot{U}) = 0\,. \tag{31}$$

Making the difference of two consecutive iterations we finally obtain, by means of eqs. (23'), (31), (24)–

(27):

$$\Delta\dot{U}^i = \hat{\mathbf{A}}^{-1}\Delta\hat{R}^i = -\hat{\mathbf{A}}^{-1}\psi^{i-1} \tag{32}$$

where:

$$\psi^{i-1} = \psi(\dot{U}^{i-1}) = \hat{R}^{i-1} - \hat{R}^i = -\Delta\hat{R}^i$$

$$= -''\sum_e ''\int_e \mathbf{B}^T\boldsymbol{\sigma}_r^i \mathrm{d}v\,, \tag{33}$$

$$\Delta\dot{U}^i = \dot{U}^i - \dot{U}^{i-1}\,;\ \Delta\hat{R}^i = \hat{R}^i - \hat{R}^{i-1}\,. \tag{34}$$

The nonlinear algebraic systems, eqs. (14) or (31), are discontinuous because of the factor μ given by eq. (17).

The iterations are stopped when the residual stresses of each element reach conveniently small values.

The adopted criterium was that, for each element,

$$\|\boldsymbol{\sigma}_{r_n}^i\| \leqslant \delta H\left(\sum_{m=1}^{n-i}\overline{\Delta\varepsilon_m^p}\right), \tag{35}$$

where the norm involved is the maximum absolute value of the components of $\boldsymbol{\sigma}_r^i$. The usual values of δ range between 0.015 and 0.005.

Once the accepted converge of the iterations is reached for the load step n, one proceeds to store the values $\Delta\boldsymbol{\sigma}_n$, ΔU_n *satisfying the equilibrium conditions*, the plastic strain $\Delta\varepsilon_n^p$, or:

$$\Delta\epsilon_{ij}^p = \tfrac{3}{2}\sigma'_{ij}\frac{\sigma'_{kl}\Delta\epsilon_{kl}}{\bar{\sigma}^2(1 + H'/3G)}\,, \tag{36}$$

and the equivalent increment of plastic strain $\Delta\bar{\varepsilon}_n^p$. Then the plasticity laws are satisfied within the error introduced by the residual stress different from zero. In this direction, preference has been given to the well established equilibrium conditions rather than the empirical laws of plasticity. The errors are better controlled by restriction (35), and for this reason such a criterion was adopted instead of the usual ones [3–5, 10, etc.].

The finite increments procedure introduces additional difficulties. The more important ones are 1) when an element enters in plasticity the increment is in general not entirely elastic nor plastic; 2) the discretized interpretation of eq. (9) originates some departures of the yield surface $F = 0$. Then, two types of corrections are implemented in the program:

1) α-correction The total increment of stress and strains of an element entering in plasticity is decomposed in purely elastic and elasto-plastic parts. The proportionality factor α of the first one is obtained as a positive root of the second degree equation:

$$0 = F(\boldsymbol{\sigma}_{n-1} + \alpha^i\mathbf{D}^{el}\Delta\boldsymbol{\varepsilon}_n^i, \kappa_{n-1}) \equiv \overline{\boldsymbol{\sigma}_{n-1} + \alpha^i\mathbf{D}^{el}\Delta\boldsymbol{\varepsilon}_n^i}$$

$$- H\left(\sum_{m=1}^{n-1}\overline{\Delta\varepsilon_m^p}\right). \tag{37}$$

For the elements which were in plasticity and are not unloaded in the present increment, α becomes zero.

2) β-correction The elasto-plastic increment of stresses

$$\Delta\boldsymbol{\sigma}^{ep} = (1 - \alpha)\,\mathbf{D}^{ep}\Delta\boldsymbol{\varepsilon}_n^i$$

is corrected to stay in the yield surface, by the factor:

$$\beta^i = \frac{H\left(\sum_{m=1}^{n-1}\overline{\Delta\varepsilon_m^p} + \overline{\Delta\epsilon_n^{p^i}}\right)}{(\overline{\boldsymbol{\sigma}^* + \Delta\boldsymbol{\sigma}^{ep}})}\,, \tag{38}$$

$$\boldsymbol{\sigma}^* = \boldsymbol{\sigma}_{n-1} + \alpha^i\mathbf{D}^{el}\Delta\boldsymbol{\varepsilon}_n^i$$

in the following way:

$$\Delta\boldsymbol{\sigma}^{ep^*} = \beta(\boldsymbol{\sigma}^* + \Delta\boldsymbol{\sigma}^{ep}) - \boldsymbol{\sigma}^*\,. \tag{39}$$

The residual stresses are now given by the expression

$$\boldsymbol{\sigma}_r^i = \beta^i(\boldsymbol{\sigma}^* + \Delta\boldsymbol{\sigma}^{ep}) - (\boldsymbol{\sigma}_{n-1} + \Delta\boldsymbol{\sigma}_n^i) = \Delta\boldsymbol{\sigma}^{ep^*} - \Delta\boldsymbol{\sigma}_n^i\,. \tag{40}$$

The appropriate formulation for the cases of plane stress, plane strain and symmetry of revolution was made in the usual manner.

The elasto-plastic matrix is evaluated for $\boldsymbol{\sigma} = \boldsymbol{\sigma}_n^{*i}$ and

$$H'\left(\sum_{m=1}^{n-1}\overline{\Delta\varepsilon_m^p}\right).$$

5. Description of the code

The fundamental steps of the program are the following:

a) Evaluate the first yield limit for loads and temperatures.

b) Evaluate incremental load and incremental temperature distribution according to the respective histories.

c) Solve the thermo-elastic incremental problem eq. (41) with initial stresses.

d) For each element make the α-adjustment, evaluate the elasto-plastic matrix, make the β-adjustment and calculate stresses.
e) Store residual stresses.
f) If the residual stresses are not small enough, go to c).
g) Store incremental stresses $\Delta\sigma_n$, plastic strains $\Delta\varepsilon_n^p$, displacements ΔU_n and $\Delta\varepsilon_n^p$.
h) Print results of the load step n.
i) If the histories of loads and temperature are not concluded, go to b).
j) END.

At each step of the load, the thermal strains $\Delta\varepsilon^\theta$ are calculated with the temperature distributions obtained with the auxiliary code "CUARM" [22], and the incremental thermo-elastic problem, eq. (17),

$$\hat{A}\Delta U = \Delta\hat{R} \tag{41}$$

is solved with some of the routines of the "ELASTEF" code [23] for general two-dimensional elastic problems. The factorization method of Cholesky is employed.

The program actually uses triangular elements with linear functions, to cover a general plane domain which can also be multiply connected. It has a total high speed memory requirement of about 100 Kbytes and it also needs disks auxiliary storage. This capacity * permits triangular nets of about 300 elements and 200 nodes. A problem of this size takes nearly 50 seconds for each iteration (steps c) to f)) excluding thermal calculations.

6. Some solved examples and discussion

With the purpose of testing the code's performance, some classical examples were solved and the results compared with those obtained by different authors.

6.1. *Perforated plate in tension*

This is a suitable example for testing numerical models and compare their predictions with the careful experimental work of Theocaris and Marketos [24]. This has been done in several papers and we take advantage of such fact including also our results.

In fig. 1 the dimension of the specimen, applied loads and the coordinate axis employed are shown. For symmetry reasons, only the shaded region of the figure was used in the calculations.

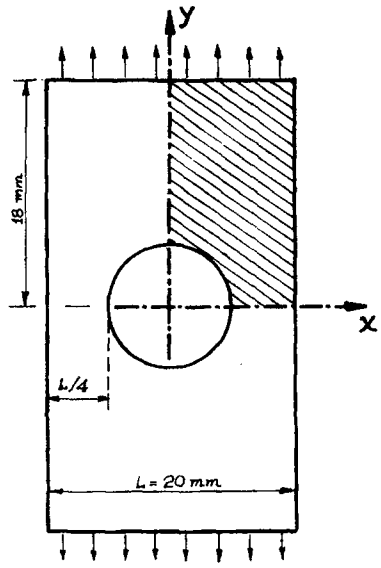

Fig. 1. Perforated plate. Dimensions of the specimen.

The material is the aluminium alloy 57S whose strain–stress curve is exhibited in fig. 2. The modulus of elasticity is E = 7000 kg/mm, being the adopted Poisson ratio ν = 0.3.

For comparative purposes, two types of results are presented: the first one obtained with the real (rounded) curve of the material as indicated in fig. 2 (from [24]) with an elastic limit strain of 0.02% (a tenth of the usual convention) and the second ones with a bilinear (sharp) approximation of this curve, also indicated

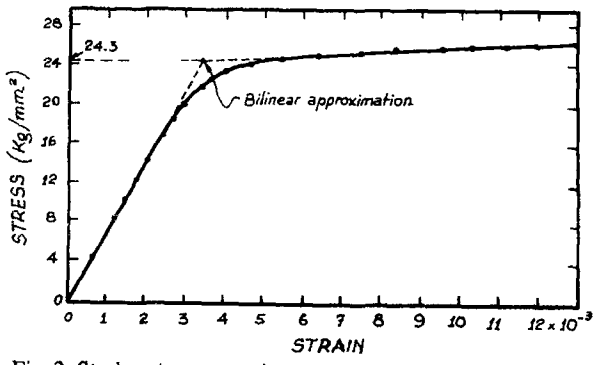

Fig. 2. Strain–stress curve in pure tension for Aluminium Alloy 57S.

* The program was implemented in the IBM/360–Mod. 44 of the Centro de Cómputos, Centro Atómico Bariloche, CNEA.

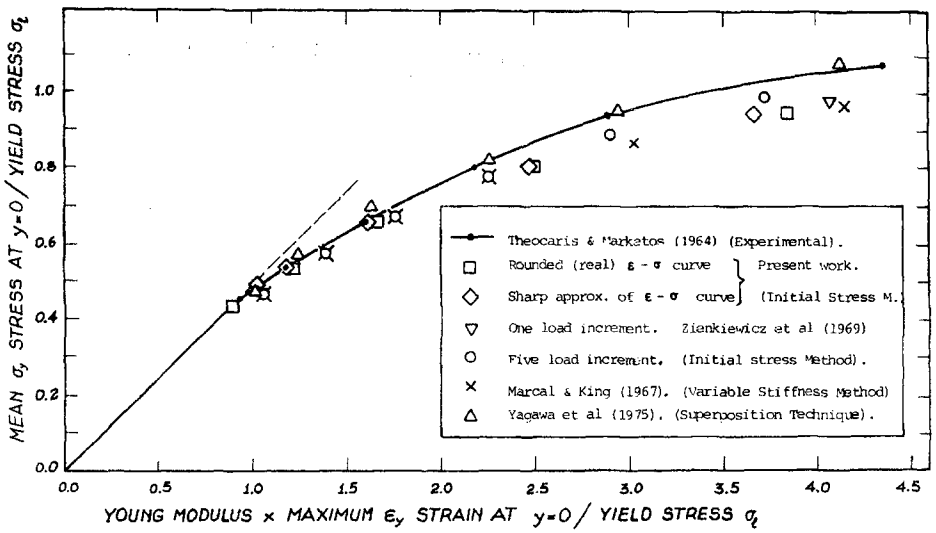

Fig. 3. Perforated plate. Maximum strain at point of first yield vs. mean stress at the section $y = 0$ (non-dimensional magnitudes).

in the figure, with a yield stress limit of 24.3 kg/mm, and a slope at the plastic region for the strain-equivalent stress curve of $H' = 225$ kg/mm^2. The originated differences, sometimes non-negligible in particular for the development of plastic enclaves, are shown in figs. 3 to 6.

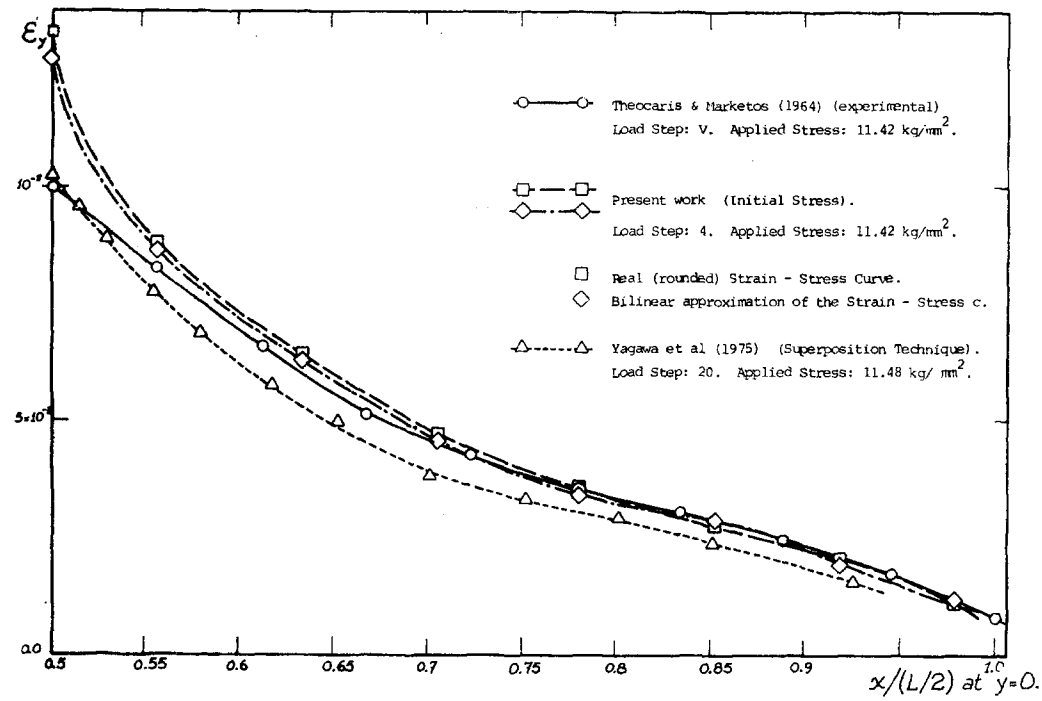

Fig. 4. ϵ_y strain distribution at the smallest section ($y = 0$) for step load 4. Comparison with experimental results and with other numerical model.

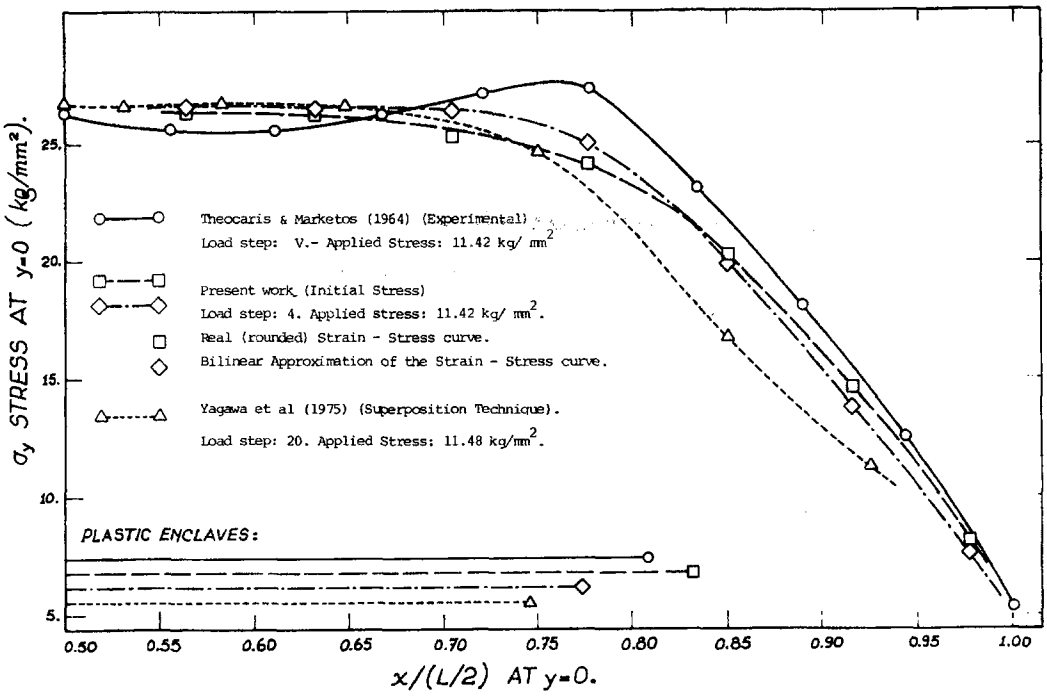

Fig. 5. σ_y stress distribution at the smallest section ($y = 0$) for step load 4. Comparison with experimental results and with other numerical model.

In fig. 3, a plot of the maximum strain at point of first yield vs. mean stress at the section $y = 0$ (homogeneous magnitudes) is presented. This curve previously used by other authors, allows for comparing different results but in our opinion has the disadvantage that this maximum strain is a rather delicate parameter, difficult to obtain in the numerical models because the strong strain gradient in this zone makes its value dependent on the local mesh size.

We observe that in general the numerical models predict a curve somewhat lower (less "rigid") than the experimental one, with the exception of the points of Yagawa et al. [8] whose model fit specially well the value of the strain just in the maximum deformation region (see fig. 4).

Our calculations were made in five load increments essentially coincident with those of Theocaris and Marketos [24], and some of those of Yagawa et al., [8]. For load step 4 (applied stress: 11.42 kg/mm), figs. 4 and 5 show a detailed comparison of the y-strain and y-stress distribution in section $y = 0$, with the experimental values [24] and disposable numerical results [8]. The agreement is very satisfactory except for ϵ_y in the left region; this automatically gives rise to some departures in fig. 3. The different plastic enclaves predicted at this stage are also indicated in fig. 5.

Finally, in fig. 6 we compare the plastic enclaves presented in the previous references with those obtained with our code. As was previously noted, this pattern is sensible to the adopted form of the strain–stress curve, near the vertex. The mesh used was that of ref. [3]. It consists of 149 triangular elements and 94 nodal points. In both cases studied the iterations were stopped with a bound $\delta = 0.005$. Each iteration takes about 23 seconds. For the first load cycles, convergence was usually reached in 3 to 15 iterations. Near the collapse it was obviously slower.

6.2. *V-notched tension specimen*

In this example a numerical simulation of a tension test for a V-notched specimen is presented. The dimensions are indicated in fig. 7. The material is supposed

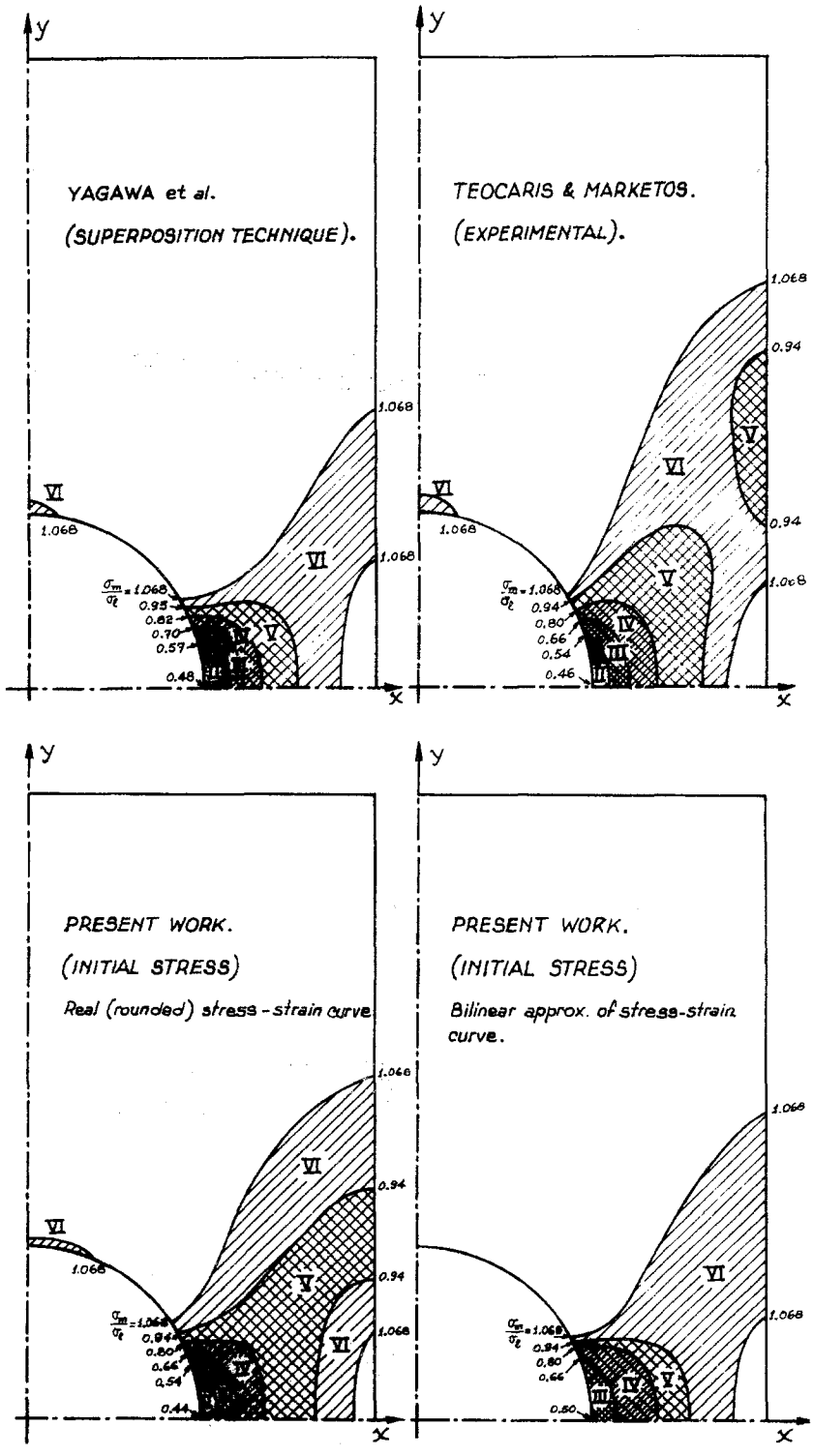

Fig. 6. Progressive yielding at perforated plate. Comparison of different results.

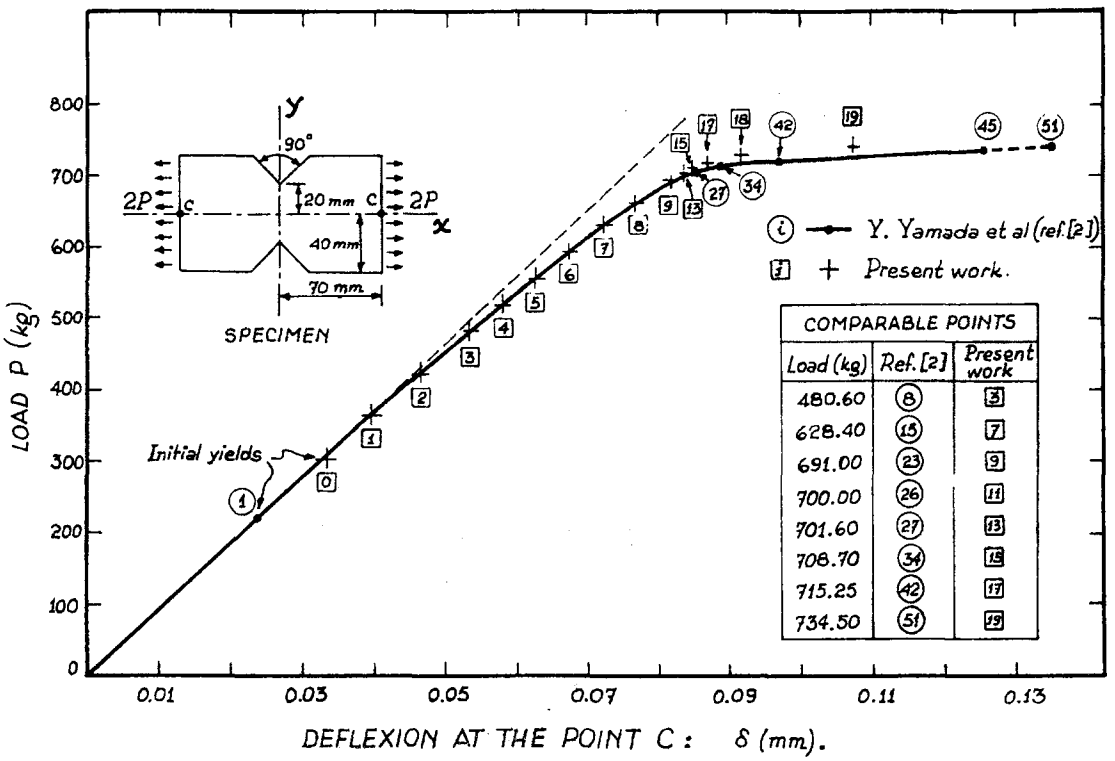

Fig. 7. Load – deflexion curve for a V-notched specimen.

to be elastic – perfectly plastic with yield stress Y = 30 kg/mm^2, Young's modulus E = 20 000 kg/mm^2 and Poisson's ratio ν = 0.3.

In fig. 7 a comparison is made of our results with those of Yamada et al. [2] for the load-deflexion curve. The deflexion considered is that of point C over the symmetry x-axis.

The correspondence is excellent except for: a) the initial yield point, and b) the final collapse stages. Case a) is to be expected because the elasticity theory predicts that for sharp notches, yielding is initiated near the notch root by the first application of load. For the finite element discretized continuum, this is then highly dependent on the mesh size near the root [2]. The agreement ceases to be satisfactory in the delicate stages near the collapse, b). A more rigid behaviour is seen in our resolution of the problem (see the comparable points of equal load in fig. 7). This was also observed when comparing both plastic enclave patterns, which nevertheless exhibit an acceptable qualitative agreement.

Variable load increments were used. At stage 19 no convergence was reached indicating the collapse of the specimen. Our predicted collapse load P_c then ranges between the values P_{18} = 724.87 kg and P_{19} = 734.50 kg, in correct agreement with that predicted by Yamada et al., coincident with the last value.

The mesh consisted of 300 triangular elements and 171 nodal points. The iterations were stopped with a bound δ = 0.01. Each iteration takes about 43 seconds.

6.3. *Simply supported rectangular beam*

A simply supported and uniformly loaded rectangular beam (fig. 8) is now studied in the elastoplastic domain, and the results compared with those of ref. [11] and the usual solution of the beam theory, for elastic – perfectly plastic materials and small h/l ratios. According to such theory, the problem is only dependent on the overload parameter $m = q/q_e$ (q = uniformly distributed load; q_e = load producing the first yield) and the ratio f/f_e of the maximum deflexion

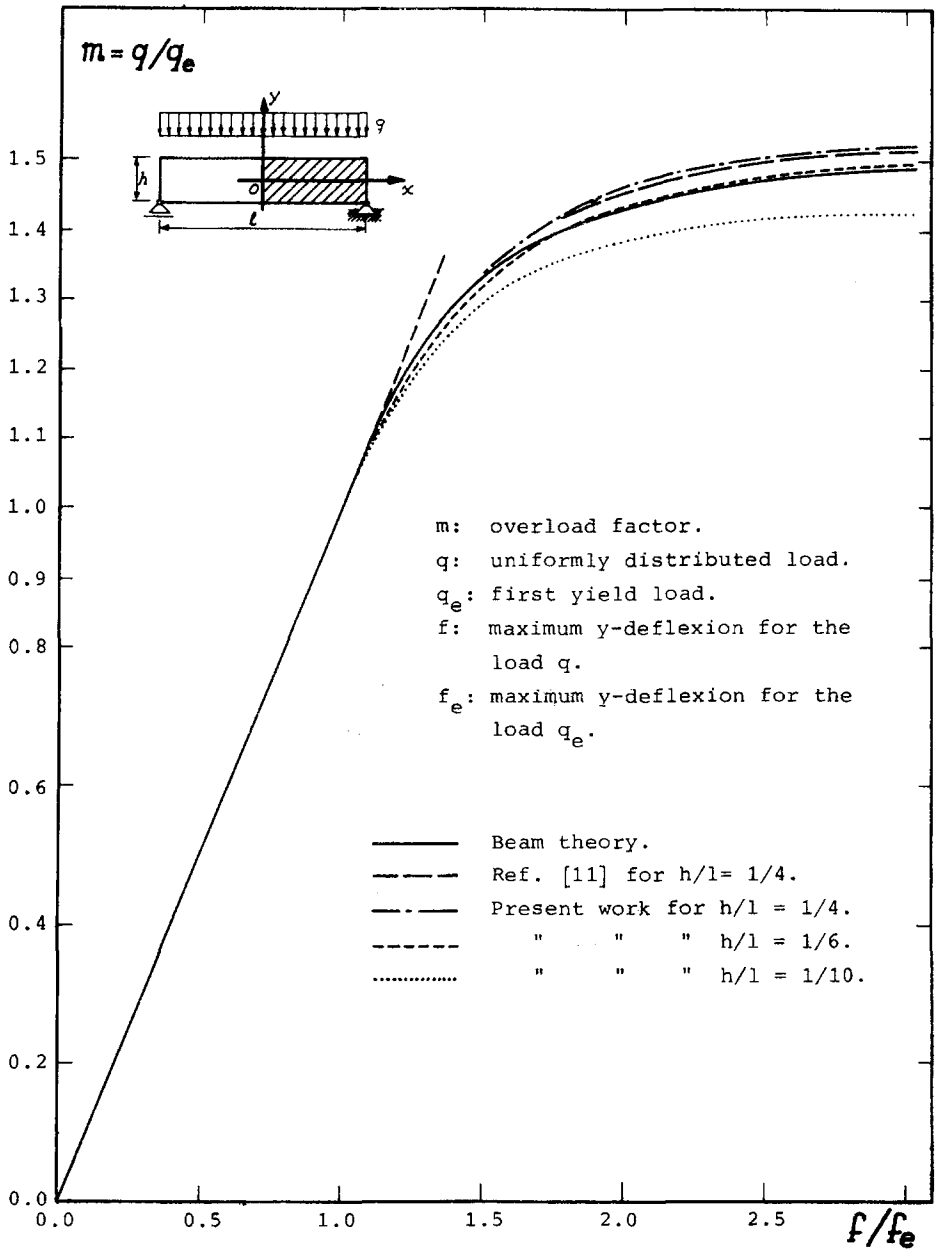

Fig. 8. Overload vs. relative maximum deflexion for a simply supported, uniformly loaded beam.

for a given load q to the maximum deflexion for the limit load q_e. The predicted collapse of the beam corresponds to $m = 1.5$.

Three numerical experiences were made for different values of the ratio h/l (1/4, 1/6 and 1/10). It is observed (fig. 8) that the results do not coincide. This feature certainly originates on the deformation caused by the tangential forces whose influence, strongly dependent on the previous ratio (ref. [24], Vol. I, p. 164), is not taken into consideration in the above mentioned theory. For example, the errors introduced for such ratios h/l in the elastic range are respectively

19.5%, 8.67% and 3.12% for a Poisson coefficient ν = 0.3. Of course the right comparison should be made for $h/l = 1/10$.

The mesh used is that of ref. [11], and consists of 256 elements and 153 nodal points. It was deformed horizontally to be adapted to the cases studied. The iterations were concluded for a bound $\delta = 0.005$.

7. Conclusions

An efficient code for the resolution of two-dimensional thermo-elastoplastic problems for general strain-hardening rules has been described, and, through some of the most representative solved examples, its satisfactory performance has been shown.

A good agreement is observed in comparison with the predictions of other numerical models and also with theoretical and experimental results, within acceptable bounds of error from a technological point of view.

The code does not require great storage capacity, nor large running time for solving standard problems accurately.

It can easily extended to permit elastic reaction boundaries, histories of imposed displacements, unhomogeneous plastic properties, etc.

Acknowledgements

The authors are very indepted to Mr. L. Arroyo and Mr. H. Cingolani * for their improvement of the code, saving a substantial amount of computer time, and to Mrs. B. Cruz *, for her help in building the finite element meshes of the test examples.

References

[1] P.V. Marcal and I.P. King, Int. J. Mech. Sci. 9 (1967) 143.
[2] Y. Yamada, N. Yoshimura and T. Sakurai, Int. J. Mech. Sci., 10 (1968) 343.
[3] O.C. Zienkiewicz, S. Valliappan and I.P. King, Int. J. Num. Meth. Eng. 1 (1969) 75.
[4] O.C. Zienkiewicz, The finite Element Method in Engineering Science (McGraw-Hill, London, 1971).
[5] G.C. Nayac and O.C, Zienkiewicz, Int. J. Num. Meth. Eng., 5 (1972) 113.
[6] K.J. Bathe, H. Ozdemir and E.L. Wilson, Rep. UCSESM No 74-4, Struct. Eng. Lab., Univ. of Calif., Berkeley, Calif., U.S.A. (1974).
[7] G. Yagawa, T. Nishioka and Y. Ando, Proc. of the 24th Japan Nat. Cong. for Appl. Mech. 13 (1974) 22.
[8] G. Yagawa, T. Nishioka and Y. Ando, Nucl. Eng. Des. 34 (1975) 247.
[9] T.H.H. Pian, R.L. Spilker and S.W. Lee, Proc. 3rd. Int Conf. on Str. Mech. in Reactor Tech., Paper M2/1* London (1975).
[10] B. Aamodt and O. Mo, Proc. 3rd. Int. Conf. on Str. Mech. in Reactor Tech., Paper M2/7 London (1975).
[11] H. Fabian, U. Krugmann, K. Lassmann and R. Schwarz, KFK 2274, Kernforschungszentrum, Karlsruhe (1976).
[12] T.R. Hsu, A.W.M. Bertels, S. Banerjee and W.C. Harrison, AECL-5233, Atomic Energy of Canada Limited, Pinawa, Manitoba (1976).
[13] F.C. Weiler, Proc. 1st. Int. Conf. on Str. Mech. in Reactor Tech., Paper D3/3 Berlin (1972).
[14] Y.R. Rashid, Nucl. Eng. Des. 29 (1974) 22.
[15] G. Yagawa and Y. Ando, Proc. 2nd. Int. Conf. on Str. Mech. in Reactor Tech., Paper L4/3, Berlin (1973).
[16] T.J. Chung and G. Yagawa, Dev. in Mech. 7 (1973) 843.
[17] Y.R. Rashid and T.Y. Chang, Proc. 1st. Conf. on Str. Mech. in Reactor Tech., Paper L4/5 Berlin (1972).
[18] Q.S. Nguyen, Int. J. Num. Meth. Eng. 11 (1977) 817.
[19] S. Nemat Nasser and M. Taya, J. of the Franklin Inst. 302 (1976) 463.
[20] R. Hill, The Mathematical Theory of Plasticity (Clarendon Press, Oxford, 1956).
[21] G. Strang, J. Franklin Inst. 302 (1976) 429.
[22] F.G. Basombrío and B. Cruz, Report CAB/1976/2, Centro Atómico Bariloche, Comisión Nacional de Energía Atómica, Argentina (1976).
[23] F.G. Basombrío and G. Sánchez, Report CNEA-NT 13/77, Comisión Nacional de Energía Atómica, Argentina (1977).
[24] P.S. Theocaris and E. Marketos, J. Mech. Phys. Solids 12 (1964) 377.
[25] S. Timoshenko, Resistencia de Materiales, Espasa-Calpe S.A., Madrid (1956).

* Centro de Cómputos, Centro Atómico Bariloche, CNEA.